Available online at www.sciencedirect.com
ScienceDirect
Carbohydrate Research 342 (2007) 2270–2285
Carbohydrate RESEARCH

DFT studies of the disaccharide, α-maltose: relaxed isopotential maps☆

Udo Schnupf,[a] J. L. Willett,[a] Wayne B. Bosma[b] and Frank A. Momany[a,*]

[a]*Plant Polymer Research, National Center for Agricultural Utilization Research, ARS, USDA, 1905 N. University St., Peoria, IL 61604, United States*
[b]*Department of Chemistry and Biochemistry, Bradley University, Peoria, IL 61625, United States*

Received 17 April 2007; received in revised form 12 June 2007; accepted 20 June 2007
Available online 3 July 2007

Abstract—The disaccharide, α-maltose, forms the molecular basis for the analysis of the structure of starch, and determining the conformational energy landscape as the molecule oscillates around the glycosidic bonds is of importance. Thus, it is of interest to determine, using density functionals and a medium size basis set, a relaxed isopotential contour map plotted as a function of the ϕ_H and ψ_H dihedral angles. The technical aspects include the method of choosing the starting conformations, the choice of scanning step size, the method of constraining the specific dihedral angles, and the fitting of data to obtain well defined contour maps. Maps were calculated at the B3LYP/6-31+G* level of theory in 5° intervals around the $(\phi_H, \psi_H) = (0°, 0°)$ position, out to ~±30° or greater, for *gg–gg′–c*, *gg–gg′–r*, *gt–gt′–c*, *gt–gt′–r*, *tg–tg′–c*, and *tg–tg′–r* conformers, as well as one-split *gg*(*c*)–*gg′*(*r*) conformer. The results show that the preferred conformation of α-maltose in vacuo depends strongly upon the hydroxyl group orientations ('*c*'/'*r*'), but the energy landscape moving away from the minimum-energy position is generally shallow and transitions between conformational positions can occur without the addition of significant energy. Mapped deviations of selected parameters such as the dipole moment; the C1–O1–C4′, H1–C1–O1, and H4′–C4′–O1 bond angles; and deviations in hydroxymethyl rotamers, O5–C5–C6–O6, O5′–C5′–C6′–O6′, C5–C6–O6–H, and C5′–C6′–O6′–H′, are presented. These allow visualization of the structural and energetic changes that occur upon rotation about the glycosidic bonds. Interactions across the bridge are visualized by deviations in H(O2)···O3′, H(O3′)···O2, and H1···H4′ distances and the H(O2)–O2–C2–C1 and H′(O3′)–O3′–C3′–C4′ hydroxyl dihedral angles. Published by Elsevier Ltd.

Keywords: Disaccharide; Maltose; Density functional; Basis set; Conformation; Isopotential relaxed maps

1. Introduction

Conformational analysis of α-(1→4)-linked disaccharides has been a subject of study for many years by a variety of computational methods, with maltose studies recently reviewed.[1] It is not our intention to present another review on the subject, but will refer to several papers closely related to the main subject of this work, that is, mapping the conformational space.[2–10] Most cited papers use classical methods,[2–7] such as molecular mechanics, with empirical force fields. However, ab initio and DFT papers have recently appeared[9–21] examining a variety of carbohydrate structural questions. Our return to mapping the model maltose system is made because of the availability of the rigorous DFT methodology, and because the energy landscape of these important carbohydrates is complicated, and understanding the structural properties of large naturally occurring amylose or starch materials is critical to the development of new materials. Relaxed isopotential maps, often called Ramachandran plots, show where regions of low energy occur in the ϕ_H and ψ_H glycosidic bonds torsional space. To be useful, these maps must be predictive and experimental structures should be found in the low-energy regions. In the calculations reported here, the

☆ Names are necessary to report factually on available data; however, the USDA neither guarantees nor warrants the standard of the product, and the use of the name by USDA implies no approval of the product to the exclusion of others that may also be suitable.

* Corresponding author. Tel./fax: +1 309 681 6362; e-mail: frank.momany@ars.usda.gov

0008-6215/$ - see front matter Published by Elsevier Ltd.
doi:10.1016/j.carres.2007.06.026

first B3LYP/6-31+G* density functional isopotential relaxed maps of α-maltose are presented. For the creation of the maps, the glycosidic dihedral angle spacing was chosen with 5° increments, ranging between ~±30° or greater around $(\phi_H, \psi_H) = (0°, 0°)$. The use of a small grid size allows use of continuous segments along an axis without the possibility of large variations in geometry that could occur as the structure is optimized with the (ϕ_H, ψ_H) dihedral constraints at the desired values. The use of the B3LYP density functional with the 6-31+G* basis set is a compromise between the preferred basis set,[1,11–20] 6-311++G**, and expediency in calculations, a result of the many points on the ϕ_H–ψ_H energy surface to be optimized, a decision made to make the connections between points interpolate smoothly. The results of these studies are presented as maps in which the deviations in the energy, and other structure-dependent parameters, are plotted as a function of the ϕ_H and ψ_H dihedral angles.

2. Experimental

2.1. Computational method

Although the basis set 6-31+G* used here is not as robust as that used 6-311++G** in previous carbohydrate optimization studies,[1,11–20] in combination with the density functional B3LYP,[22] it is fully adequate to prepare high-quality (ϕ_H, ψ_H) isopotential contour maps where the magnitude of the energy contours falls within a few kcal/mol of the minimum energy, and explicit water molecules are not involved.[19] The basis set relative energy differences were examined previously[19] for the monosaccharide allose and showed only small deviations between the relative energies obtained with the 6-311++G** and 6-31+G* basis sets. Further, energy comparisons taken from the work of Momany et al.[1] are shown here for α-maltose in Figure 1. Figure 1 shows that the deviation in relative energies (ΔE) of the two basis sets are generally within several tenths of a kcal/mol of one another for α-maltose, as indicated by the slope of the fitted line being close to 1.

Parallel Quantum Solutions[23] software and hardware (QS8-2400S, and QS16-2000S) were utilized throughout for (ϕ_H, ψ_H) constrained energy optimization at each point on the isopotential ϕ_H–ψ_H map. Convergence criteria were similar to those used for previously published saccharides[1,11–21] with an energy change of less than 1×10^{-6} Hartree and a gradient of less than 3×10^{-4} a.u. The computed Hessians during optimization did not show negative eigenvalues, indicating that the optimized structure is at a local minimum under the given (ϕ_H, ψ_H) dihedral constraint. Results have been displayed using HYPERCHEM[24] v7.5 and ORIGIN[25] v7.5, with the contour maps created by interpolative methods between grid points. The standard numbering scheme for sugars was used and is displayed for clarification in Figure 2.

2.2. Isopotential and isogeometric contour maps

From previous[1] DFT optimization studies of α-maltose conformations, it is clear that several different exocyclic

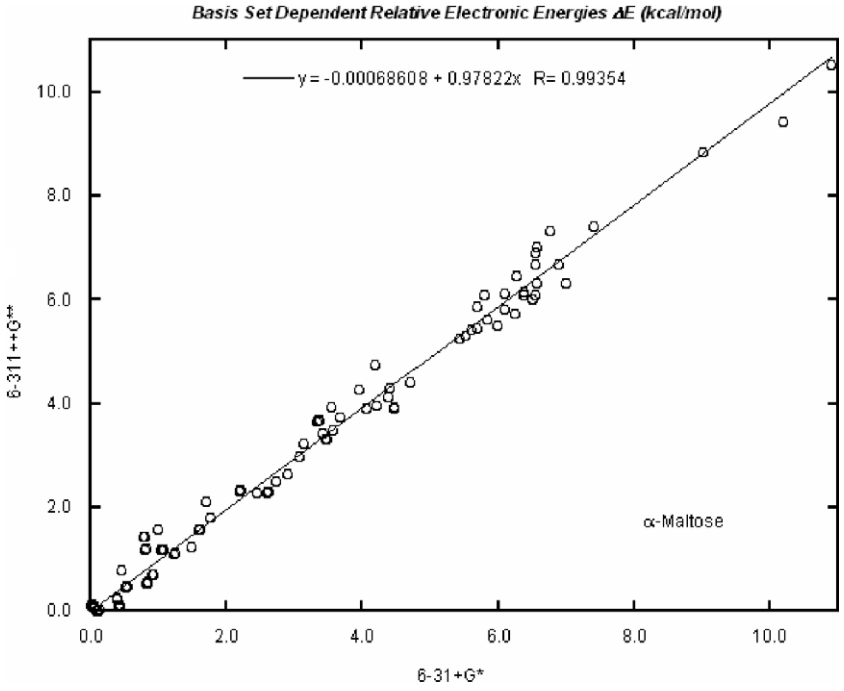

Figure 1. Plot of optimized relative electronic energies ΔE (kcal/mol) of α-maltose conformations for B3LYP/6-311++G** versus B3LYP/6- 31+G*.

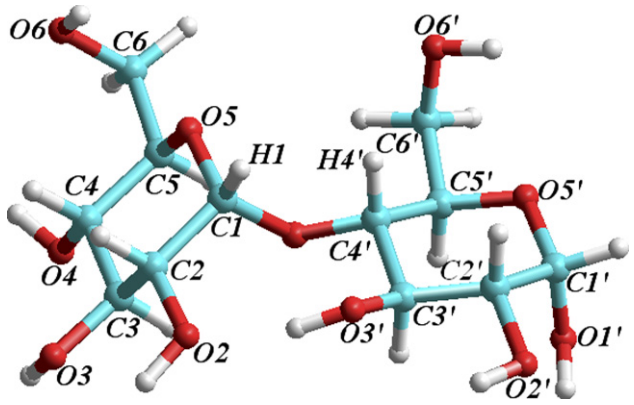

Figure 2. Numbering scheme.

conformations are of interest to map. These include the clockwise or '*c*' form and the counterclockwise or '*r*' form of the hydroxyl groups for each of the *gg–gg′*, *gt–gt′*, and *tg–tg′* hydroxymethyl group conformations. It is important to note that the hydroxymethyl group position on the reducing residue is quite important in describing the shape of the map only when in the high-energy *tg′* conformation, with the hydroxymethyl group on the non-reducing end playing a minor role when either *gg* or *tg*. We choose to study only the conformational combinations mentioned above, noting that other hydroxymethyl combinations such as *tg–gt′*, would result in a map that is very similar to a *gg–gt′* map, or for that matter, a *tg–gg′* map. Similarly, little new information would arise from maps of other missing hydroxymethyl combinations, as shown previously.[3]

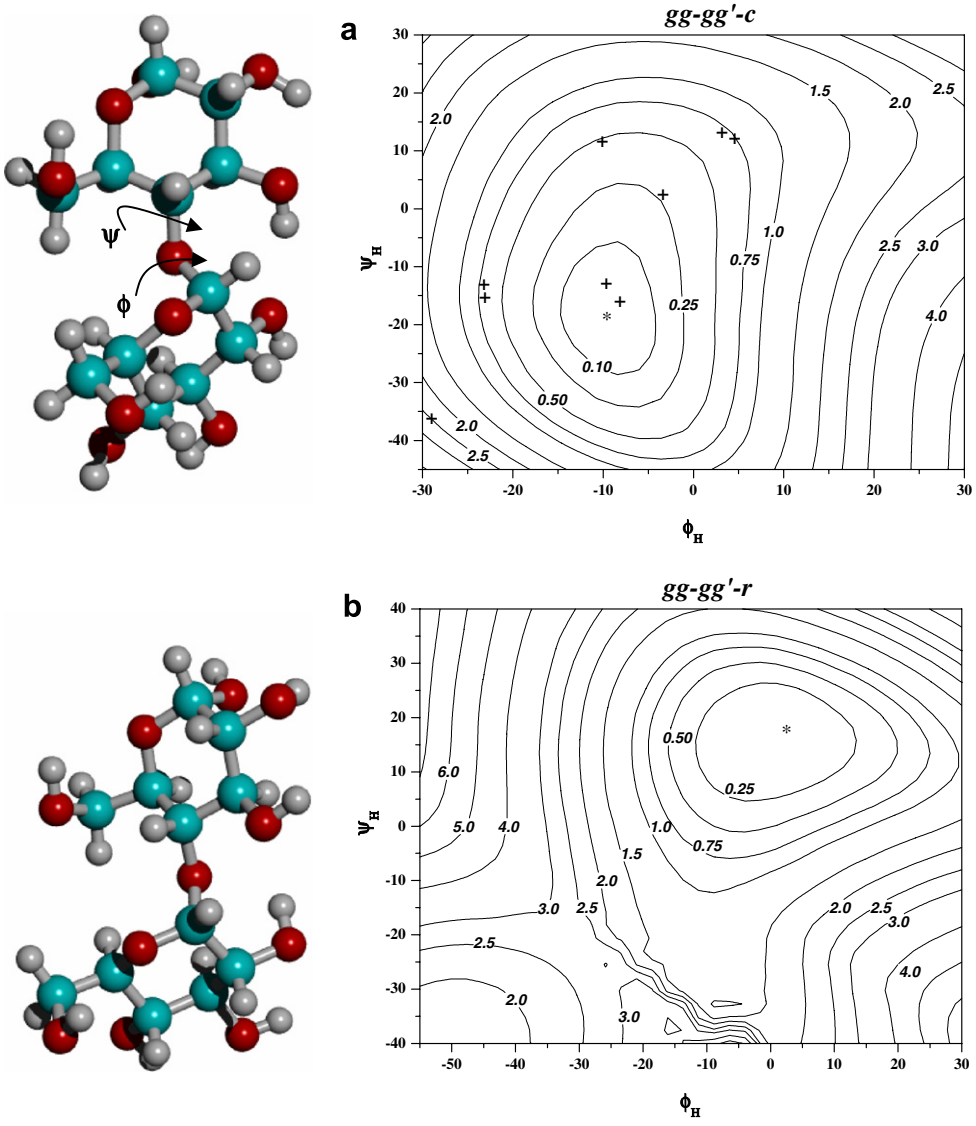

Figure 3. Relaxed isopotential (ϕ_H, ψ_H) maps for the *gg–gg′–c* and *gg–gg′–r* conformation of α-maltose. The contour line values are in kcal/mol and are relative to the lowest energy point of *gg–gg′–c* (a) $E = -814487.374$ kcal/mol and *gg–gg′–r* (b) $E = -814487.405$ kcal/mol, respectively. In (a) several experimental (ϕ_H, ψ_H) values are superimposed and denoted as '+'. The experimental values were taken from Ref. 1, Table IV.

In addition, a split hydroxyl direction case, $gg(c)$–$gg'(r)$, in which the 'c' and 'r' hydroxyl directions oppose each other, is mapped and covers a broad conformational space.

The appropriate H6–O6–C6–C5 starting dihedral angles (and their primed equivalents) are chosen from previously published work.[1,11] Thus the variation in the above dihedral and other structural parameters can be described by a geometry difference map similarly to the energy difference map. The use of primes on the reducing end is chosen to be consistent with a majority of conformational papers on maltose.[1]

Each map is made from at least a 13×13 grid reflecting a $\pm 30°$ map in ϕ_H and ψ_H with 5° increments. Maps of the 'r' conformers have expanded grid sizes to cover regions of conformational space not included in the $\pm 30°$ maps, to include 'kink' conformers.[1] During the steps between points on the map, the glycosidic linkage torsion dihedral angles are constrained to take the desired values, while all other internal coordinates are allowed to move upon energy optimization. This optimization step defines a point on the relaxed map.

The energy maps contain minimum-energy positions located in two different conformational regions around $(\phi_H, \psi_H) = (0°, 0°)$, that is, in the $(+,+)$ and $(-,-)$ regions, as found from previous optimization studies.[1,11] The method used to start the scan must be carefully defined, and for this we choose the appropriate minimum-energy structure for each map from recent studies.[1,11] Upon incrementing the specified glycosidic dihedral angle, the previously energy-minimized constrained structure in the array sequence is used for the

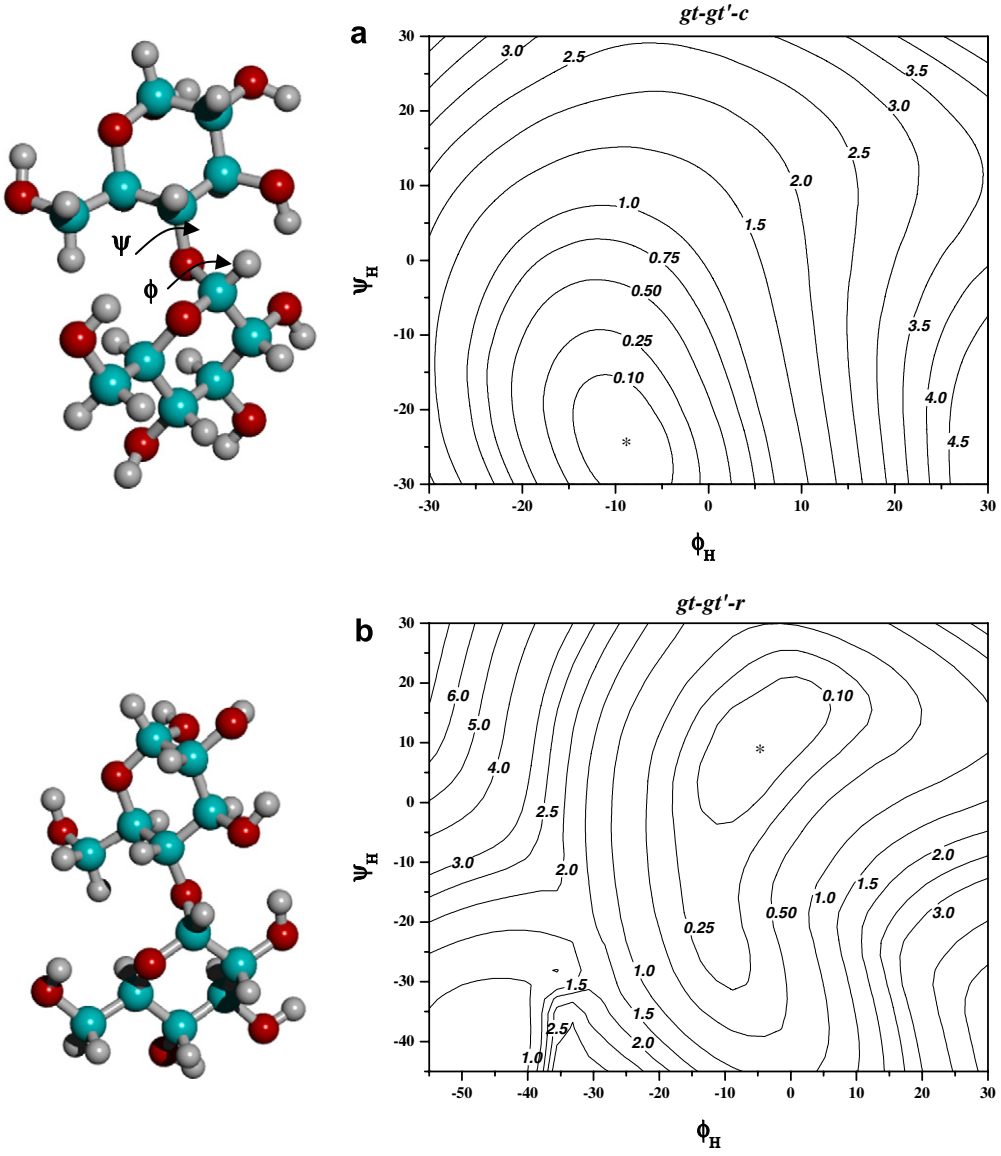

Figure 4. Relaxed isopotential (ϕ_H, ψ_H) maps for the gt–gt'–c and gt–gt'–r conformation of α-maltose. The contour line values are in kcal/mol and are relative to the lowest energy point of gt–gt'–c (a) $E = -814485.195$ kcal/mol and gt–gt'–r (b) $E = -814486.220$ kcal/mol.

next starting structure. In order for this process to be successful, the incremental steps in dihedral angles are kept small, that is, at 5°, a relatively small step size, and one during which no major geometry variation is expected to occur between steps. In those regions of conformational space where both high energy and large structural changes occur, such as rotation of a hydroxymethyl group to a new position (i.e., *tg′* to *gt′*), the map is blocked out. Internal coordinates were examined at each point after optimization in order to confirm that no major conformational changes occurred. Because of the small step size used, interpolation between points to create the isopotential maps is relatively straightforward. Although it has been argued[26] that one should use the heavy atoms to define the constrained dihedral angles, it was not found necessary in this work since the H1 and H4′ hydrogen positions were defined exactly at each point, and the optimization of all the atoms converged successfully at each point on the isopotential map. It was perhaps helpful that very high-energy regions of space were not often examined in this analysis, since major distortions in geometry can occur at the high-energy regions of conformational space.

Maps over the dihedral angle space of changes in selected internal coordinate are also presented. In particular, the ϕ_H–ψ_H map plotting the deviations of the bond angles, C1–O1–C4′, H1–C1–O1, and H4′–C4′–O1, as well as the deviations in hydroxymethyl dihedral angles, $\chi 1$ and $\chi 2$, the H6–O6–C5–C4 and the primed atoms' dihedral angle variations. Together with the dihedral difference maps for the hydroxyl groups across the glycosidic bridge, a map of the non-bonded distance between the atoms (H′(O3′)···O2, H(O2)···O3′) and H1···H4′ taking part in the hydrogen bond across the

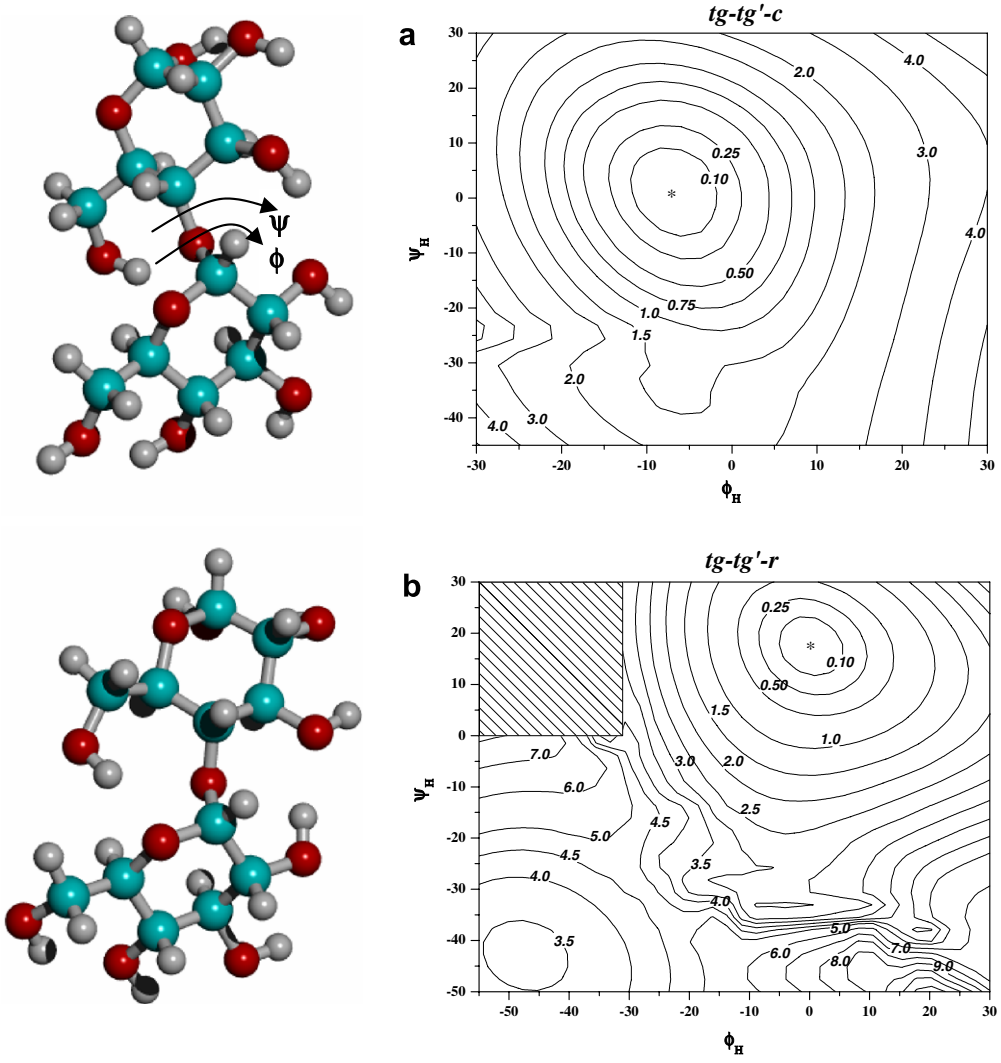

Figure 5. Relaxed isopotential (ϕ_H, ψ_H) maps for the *tg–tg′–c* and *tg–tg′–r* conformation of α-maltose. The contour line values are in kcal/mol and are relative to the lowest energy point of *tg–tg′–c* (a) $E = -814486.085$ kcal/mol and *tg–tg′–r* (b) $E = -814487.005$ kcal/mol. The marked out area in Figure 4b is a high-energy region in which conformational changes take place.

glycosidic bond is also created. The deviations in net dipole moment were mapped, using as a base value in each case, the individual value for the conformer at the lowest energy grid point on the map. The base value of these internal coordinates is the value at the lowest energy map point, and may not be the same as that found for the absolute minimum-energy conformation, but because the step sizes are small, it will be very close to the fully optimized value for this basis set.

3. Results and discussion

Relaxed ϕ_H–ψ_H isopotential B3LYP/6-31+G* energy maps are shown in Figures 3–6. Several experimental ϕ_H–ψ_H values[1] are superimposed on the *gg*–*gg*′–*c* (Fig. 3a) map and are found to fall generally in low-energy regions of the maps.

It is clear from the isopotential maps that there are significant differences between low-energy regions of the *gg*–*gg*′–*c* map (Fig. 3a) and the *gg*–*gg*′–*r* map (Fig. 3b), with the '*c*' form having a low-energy region in the negative or ~(−10°, −20° to −25°) region of ϕ_H–ψ_H space for both *gg*–*gg*′ and *gt*–*gt*′ (Figs. 3a and 4a), while the '*r*' (Figs. 3b and 4b) forms show that the low-energy region is in the positive or ~(+5°, +10° to +20°) region of ϕ_H–ψ_H space. It is also apparent that most of the experimental structures (see Fig. 3a) are located in the regions of low energy, with the exception of heavily substituted derivatives of α-maltose, which apparently create sufficient stress on the glycosidic dihedral angles that the rings are twisted out of the lowest energy regions. It was shown previously[1] that when the α-maltose '*c*' conformations were optimized starting from the region of conformational space with dihedral angles larger than ±30°, they always return to the low-energy region shown in Figures 3a and 4a. On the other hand, the *gg*–*gg*′–*r* and *gt*–*gt*′–*r* conformers show a second minimum-energy conformation outside the ±30° grid, at ~(−50°, −40°), making it necessary to expand the grid space as shown (Figs. 3b and 4b). The second minimum-energy region is denoted by a 'kink' conformation, and occurs only when all the hydroxyl groups are in the '*r*' direction around both rings, that is, this is not a region of minimum energy for '*c*' conformers.

From some previously published[2–7] (empirical) conformational studies (see Table IV in Ref. 1 for a more complete listing), in which very large positive and negative values of ϕ_H and ψ_H were reported as energy minima, it seems reasonable to assume that the empirical force fields used produced low-energy conformational artifacts that are only available for highly substituted structures in which stress energy overcomes the rotational barriers or for those cases in which the ring-to-ring hydrogen bonding is unavailable. The overall shape of the maps agree with empirical studies[2–7] where a comparison can be made, while the slope of the energy as one moves away from the minimum-energy position, is very different, being much softer than the empirical potentials. Many MM3 maps have been published (see Ref. 7 as an example), and the general shape of the maps so calculated are similar to the DFT maps, with their energy minimum being on the average shifted by ~25° or more ($\phi_H = -40°$, $\psi_H = -40°$) away from the DFT minima found here. The force field, CHEAT95[5] gives values for maltose energy minima of ($\phi_H = -70°$, $\psi_H = -44°$) and ($\phi_H = -11°$, $\psi_H = 37°$), presenting the first or 'kink' structure as the lowest energy conformation. This would not be in agreement with the DFT results.[1] Perhaps the closest empirical study to our

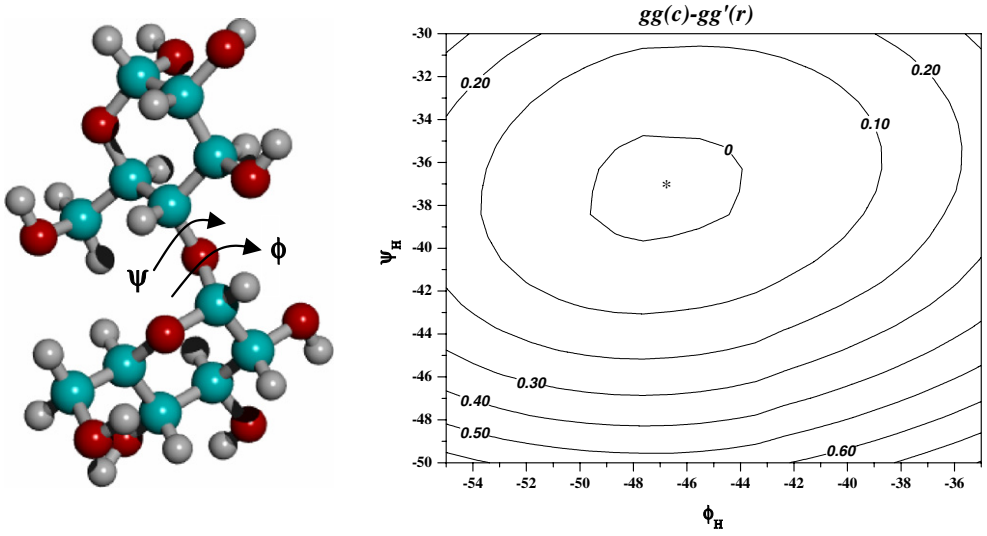

Figure 6. Relaxed isopotential (ϕ_H, ψ_H) map for the *gg*(*c*)–*gg*′(*r*) conformation of α-maltose. The contour line values are in kcal/mol and are relative to the lowest energy point of *gg*(*c*)–*gg*′(*r*) $E = -814483.323$ kcal/mol.

DFT results is the CHARMM/CSFF map[2] with the global minimum-energy position of ($\phi_H = -24°$, $\psi_H = -22°$). Unfortunately, it is difficult to separate out of their work,[2] the '*c*/*r*' differences described in this work, so even though the maps appear similar to ours in shape, the energy differences may not agree very closely. By combining all conformations into a total adiabatic map, one hides the individual contributions from different hydroxyl rotamers, making comparisons difficult.

The *tg*–*tg*′–*c* and *tg*–*tg*′–*r* isopotential maps are shown in Figure 5a and b. In both figures the area of the map with energy lower than the 1 kcal/mol contour is sharply reduced relative to the previous *gg*–*gg*′ and *gt*–*gt*′ maps. When the area of low energy is reduced, as shown in Figure 5, it suggests that both the entropy as well as higher energy will combine to lower the probability of occurrence of the *tg*–*tg*′ hydroxymethyl conformations. This is not to say that a *tg*-bearing residue at the non-reducing end of a polymer chain would not have the *tg* conformation. On the contrary, *tg* may be a favored conformer at that position[1] and possibly around band-flip conformations. As before for *gg*–*gg*′–*r* and *gt*–*gt*′–*r* a 'kink' local energy minimum is found, being several kcal/mol higher in energy than the lowest energy position on the map, see Figure 5b. A region of conformational space in which the hydroxymethyl rotamers changed state is blocked out in the upper left corner of Figure 5b.

In Figure 6 the ϕ_H–ψ_H map (note that the scale is changed on the figure) for the split conformational

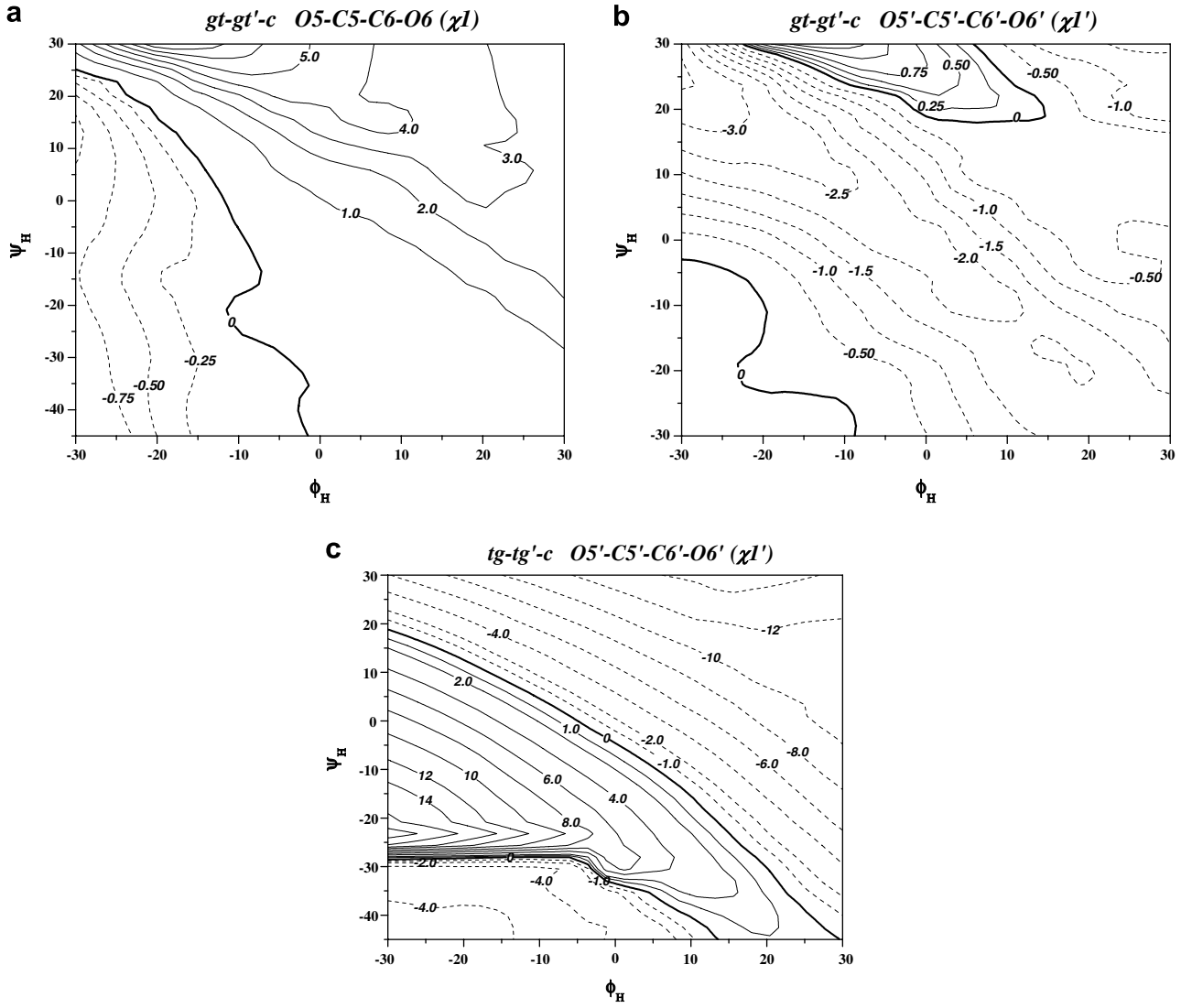

Figure 7. Isogeometric (ϕ_H, ψ_H) maps for the O5–C5–C6–O6 and O5′–C5′–C6′–O6′ dihedral angles: (a) Relative O5–C5–C6–O6 dihedral angle (°) as a function of (ϕ_H, ψ_H) for the *gt*–*gt*′–*c* conformation of α-maltose with respect to the value of 60.3°, at the lowest energy point (see Fig. 3a). (b) Relative O5′–C5′–C6′–O6′ dihedral angle (°) as a function of (ϕ_H, ψ_H) for the *gt*–*gt*′–*c* conformation of α-maltose with respect to the value of 61.8°, at the lowest energy point (see Fig. 3a). (c) Relative O5′–C5′–C6′–O6′ dihedral angle (°) as a function of (ϕ_H, ψ_H) for the *tg*–*tg*′–*c* conformation of α-maltose with respect to the value of 168.8°, at the lowest energy point (see Fig. 4a).

form, $gg(c)$–$gg'(r)$, is shown. The dramatic move of the minimum-energy position to $(\phi_H, \psi_H) \sim (-47°, -43°)$ or the 'kink' region of space is consistent with optimization results of Ref. 1. Figure 6 shows that this structure is very flexible, being able to move 20° or more in either the ϕ_H or ψ_H direction without large variation in energy. It must be noted that this minimum-energy position is of much higher relative energy of ~4 kcal/mol compared to the *gg*–*gg′*–*c* or *gg*–*gg′*–*r* minimum-energy structures, and thus is not of great interest in the vacuum state. However, it remains to be seen if this state can be found during simulations with solvent. Preliminary results from DFT ab initio molecular dynamics simulations, using COSMO[27] as a solvent simulation tool, do not show a tendency toward this conformational state.[28]

3.1. Hydroxymethyl rotamers deviations

The two rotamers defined by atoms O5–C5–C6–O6 ($\chi 1$) and O5′–C5′–C6′–O6′ ($\chi 1'$) differ as shown in the *gt*–*gt′*–*c* maps of Figure 7a and b. It is clear that some stress is placed on the $\chi 1$ rotamer (Fig. 7a) which shows deviations of ~5° or less, while the primed or $\chi 1'$ rotamer (Fig. 7b) shows deviations of up to 3°. As one moves away from one 0° deviation line, shown in the upper middle region of the map as well as the lower left region of Figure 7b, the variation in $\chi 1'$ shows a decided shape

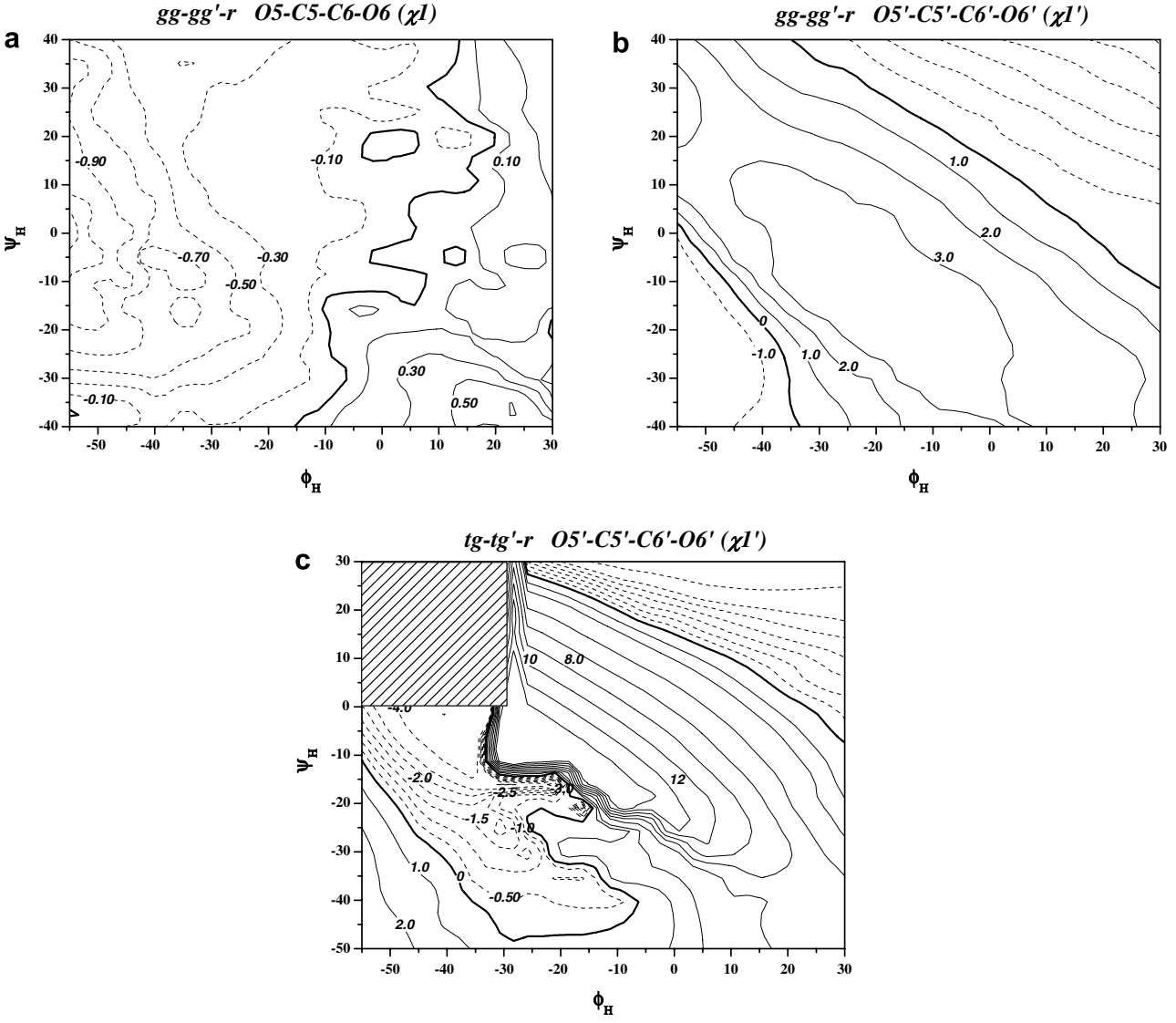

Figure 8. Isogeometric (ϕ_H, ψ_H) maps for the O5–C5–C6–O6 and O5′–C5′–C6′–O6′ dihedral angles. (a) Relative O5–C5–C6–O6 dihedral angle (°) as a function of (ϕ_H, ψ_H) for the *gt*–*gt′*–*r* conformation of α-maltose with respect to the value of −57.3°, at the lowest energy point (see Fig. 3b). (b) Relative O5′–C5′–C6′–O6′ dihedral angle (°) as a function of (ϕ_H, ψ_H) for the *gt*–*gt′*–*r* conformation of α-maltose with respect to the value of −61.9°, at the lowest energy point (see Fig. 3b). (c) Relative O5′–C5′–C6′–O6′ dihedral angle (°) as a function of (ϕ_H, ψ_H) for the *tg*–*tg′*–*r* conformation of α-maltose with respect to the value of 157.9°, at the lowest energy point (see Fig. 4b).

difference when compared to the $\chi 1$ dihedral angle map in Figure 7a. It is of special interest that even when the ϕ_H and ψ_H dihedral angles move by 10–20° away from the -0- deviation line(s), there is only a 1–3° variation in $\chi 1$ or $\chi 1'$. This is very useful information since it implies that no serious stress is placed on these dihedral angle variables as the glycosidic bonds rotate about their minimum-energy values. It also suggests that fairly large variations in ϕ_H and ψ_H do not impose large changes in these internal coordinates, which is in accord with the shallow gradient of the energy maps.

The *tg–tg′–c* map of $\chi 1'$ is significantly different than those described above (see Fig. 7c). With variations of more than 10° at many places on the map, it suggests a much tighter region in conformational space where fluctuations can take place without serious energy deviations. The region of variation on each side of the diagonal -0- deviation line quickly becomes large changing by ~4° within a change of ~10° in ϕ_H–ψ_H space.

The *gg–gg′–r* maps of $\chi 1$ and $\chi 1'$ are similar to the *gg–gg′–c* maps in magnitude of variation but not shape, as shown in Figure 8a and b. The $\chi 1'$ map shows

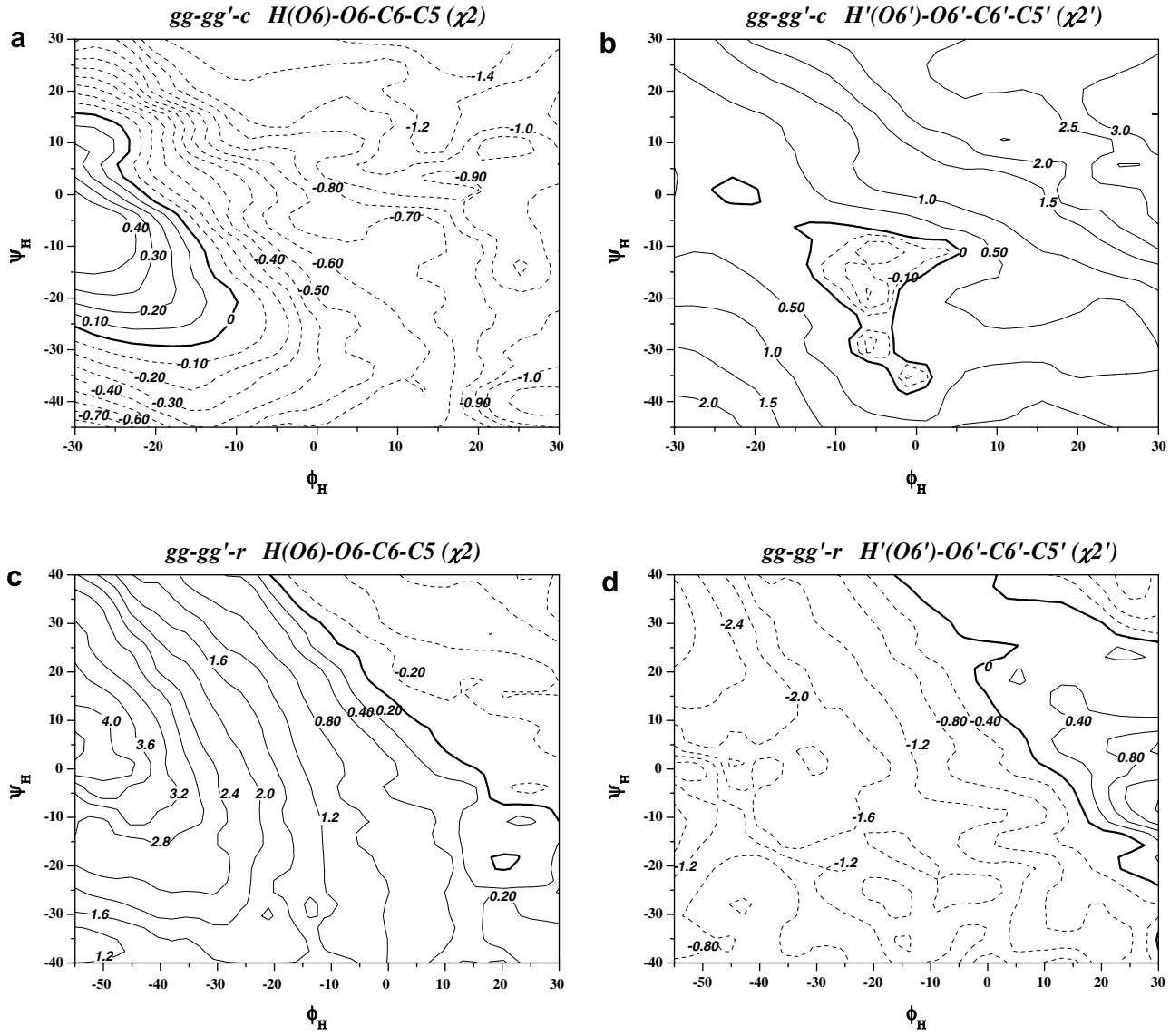

Figure 9. Isogeometric (ϕ_H, ψ_H) maps for the H(O6)–O6–C6–C5 and H′(O6′)–O6′–C6′–C5′ dihedral angles. (a) Relative H(O6)–O6–C6–C5 dihedral angle (°) as a function of (ϕ_H, ψ_H) for the *gg–gg′–c* conformation of α-maltose with respect to the value of 63.1°, at the lowest energy point (see Fig. 2a). (b) Relative H′(O6′)–O6′–C6′–C5′dihedral angle (°) as a function of (ϕ_H, ψ_H) for the *gg–gg′–c* conformation of α-maltose with respect to the value of 57.9° at the lowest energy point (see Fig. 2a). (c) Relative H(O6)–O6–C6–C5 dihedral angle (°) as a function of (ϕ_H, ψ_H) for the *gg–gg′–r* conformation of α-maltose with respect to the value of 56.2°, at the lowest energy point (see Fig. 2b). (d) Relative H′(O6′)–O6′–C6′–C5′ dihedral angle (°) as a function of (ϕ_H, ψ_H) for the *gg–gg′–r* conformation of α-maltose with respect to the value of 61.9°, at the lowest energy point (see Fig. 2b).

somewhat larger deviations than the $\chi 1$ map, but the deviations are small. Positive and negative variations occur in both maps, and the $\chi 1'$ map -0- deviation line extends across the whole $\pm 30°$ map with positive deviation values of $\sim 2°$. The *tg–tg′–r* $\chi 1'$ map (see Fig. 8c) shows catastrophic changes with only slight variance in ϕ and ψ.

It is of interest that in both the *gg–gg′–c* and *gg–gg′–r* relative energy maps the (0,0) region is only ~0.5 kcal/mol higher in energy than the minimum-energy conformation, indicating a small energy barrier in going from the $(-,-)$ region of conformational space to the $(+,+)$ region, if the exocyclic hydroxyl groups were to rotate from the '*c*' to the '*r*' conformation while the glycosidic bond was undergoing this transition. In a larger polymer this transition would be of higher energy (see Table I of Ref. 1), a result of the hydroxyl groups now pointing at the hydrogen atoms of a residue that did not undergo the rotation. This suggests that a cooperative motion must occur along a chain in order for this rotational event to occur. In the event the molecules were solvated, this rotational motion could occur more easily since the hydroxyl groups would be pointed more outward toward the solvent and be more easily rotated to a new conformation.

The deviations from the lowest energy grid points of the hydroxymethyl rotamers defined by the atoms H(O6)–O6–C6–C5 ($\chi 2$) and the H′(O6′)–O6′–C6′–C5′ ($\chi 2'$) atoms are shown in Figure 9a–d for the *gg–gg′–c* and '*r*' maps. Again, the changes that occur upon variation in ϕ_H and ψ_H are small overall, indicating that the $\chi 2$ and $\chi 2'$ dihedral angles of the hydroxymethyl groups do not change significantly upon change in glycosidic bond dihedral angles. There are significant differences between the *gg–gg′–c* and '*r*' maps, with the '*r*' maps having a -0- deviation line running nearly vertically across the map in both hydroxymethyl H–O–C–C rotamers, while the '*c*' maps do not, being more complex but still with small deviations.

The maps of H(O6)–O6–C6–C5 and the primed form for the *gt–gt′–c* and '*r*' cases are similar to those above and are not shown. Clearly, there are two flexible dihedral angles $\chi 1$ and $\chi 2$ that can undergo variation for each hydroxymethyl rotamer, and it appears that when one changes the other tends to compensate to minimize the energy change, as expected.

The difference maps for the two hydroxyl groups involved in hydrogen bonding across the glycosidic bonds are shown in Figure 10a and b for the *gg–gg′* conformers. In the *gg–gg′–c* form, the H′(O3′)-hydroxyl hydrogen points toward the O2-oxygen, and as ϕ_H and ψ_H are rotated, the H′(O3′)–O3′–C3′–C4′ dihedral angle must rotate to optimize the interaction energy (see Fig. 10a). In the case of the '*r*' form, the H(O2)-hydroxyl hydrogen atom points toward the O3′-oxygen, and again this group must follow the direction of O3′–by rotating the H(O2)–O2–C2–C1 dihedral angle as the glycosidic bonds are varied. Variance in this dihedral angle with glycosidic dihedral angles variation is shown in Figure 10b.

The two cases described above pose the most serious variance measures of all the internal coordinates studied, with variations from $-70°$ to $+70°$, respectively. If changes of more than $\sim 60°$ are found, it is clear that the definition of '*c*' and '*r*' must be examined; however, when one hydroxyl group moves by this amount it may

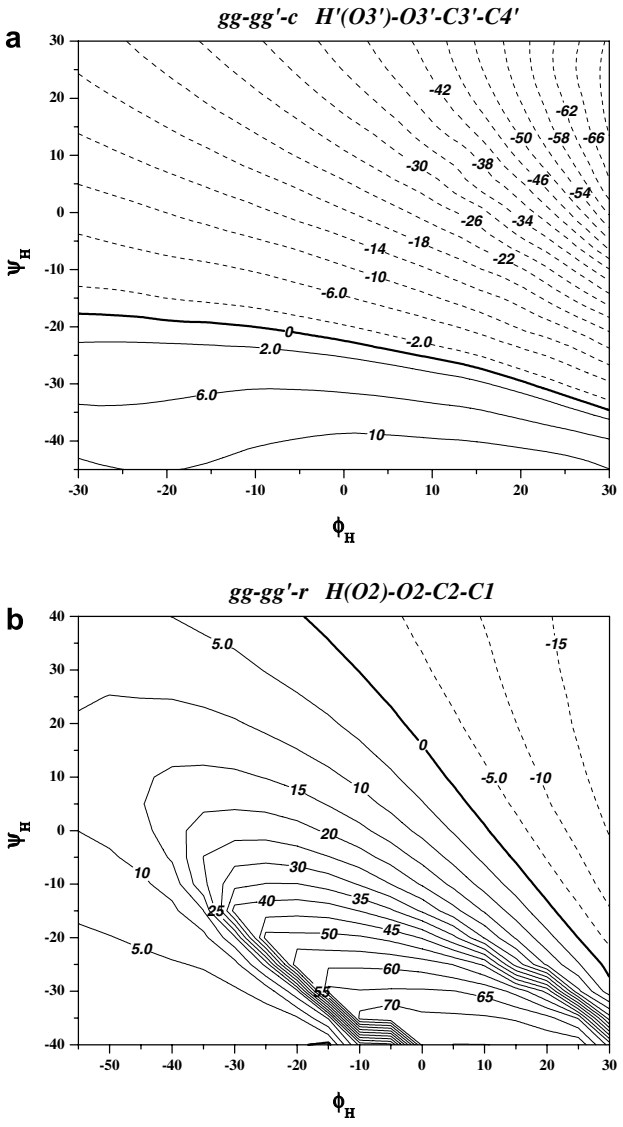

Figure 10. Isogeometric (ϕ_H, ψ_H) maps for the H′(O3′)–O3′–C3′–C4′ and H(O2)–O2–C2–C1 dihedral angles: (a) Relative H′(O3′)–O3′–C3′–C4′ dihedral angle (°) as a function of (ϕ_H, ψ_H) for the *gg–gg′–c* conformation of α-maltose with respect to the value of 70.5° at the lowest energy point (see Fig. 2a). (b) Relative H(O2)–O2–C2–C1 dihedral angle (°) as function of (ϕ_H, ψ_H) for the *gg–gg′–r* conformation of α-maltose with respect to the value of $-13.4°$, at the lowest energy point (see Fig. 2b).

still point in a clockwise or counterclockwise direction. For example in the '*c*' case, when the ϕ_H dihedral angle moves positively from ~0° out to ~+30°, the O3′-hydroxyl group varies by ~−60°, moving from ~+60° to ~0°. On the other hand, in the '*r*' form, an O2-hydroxyl group moves from a dihedral angle value of ~−60° to ~0° as ψ_H rotates from ~+20° to −40°. That these large variations in hydroxyl rotation occur as a result of interactions across the glycosidic bond with only small energy changes (~2.5 kcal/mol) suggests that it is primarily the intrinsic barrier to hydroxyl rotation that increases the relative energy as the dihedral angle approaches 0° and not some other forces.

3.2. Bond angles

In order to test some internal coordinates' stress as the glycosidic dihedral angles are twisted, three different bond-angle deviations located on the glycosidic atoms (C1–O1–C4′, H1–C1–O1, H4′–C4′–O1) were mapped, with the deviations taken from the angle values at the lowest energy map point being taken as the base values. Figures 11a–c and 12a–c show deviations in the angles noted above for *gg–gg′–c* and *gg–gg′–r*, respectively. The figures are very similar for the same internal coordinate, with two -0- deviation lines, just moved to different positions on the map from the difference in '*c*' and '*r*'

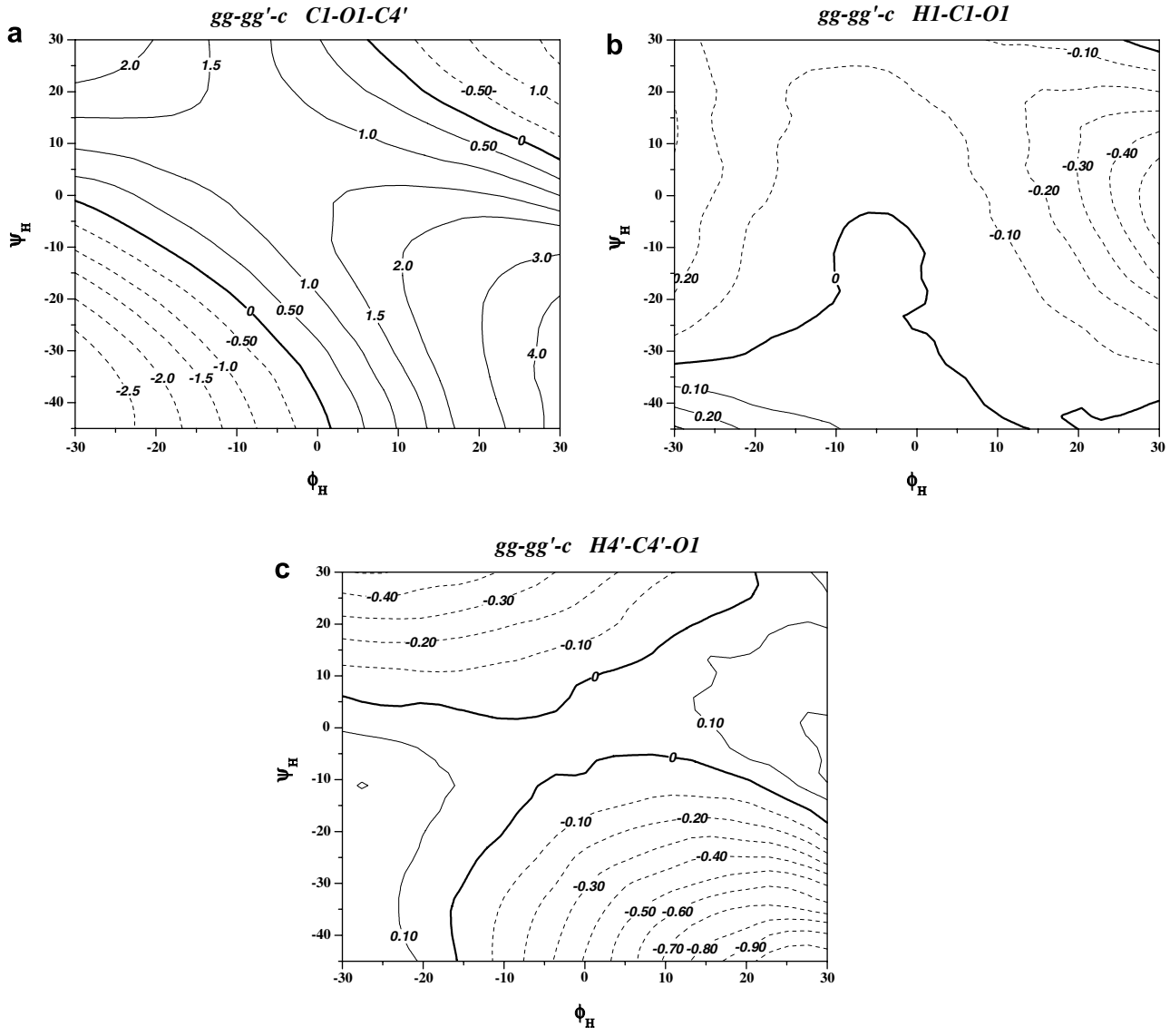

Figure 11. Isogeometric (ϕ_H, ψ_H) maps for the C1–O1–C4′, H1–C1–O1, and H4′–C4′–O1 angles. (a) Relative C1–O1–C4′ angle (°) as a function of (ϕ_H, ψ_H) for the *gg–gg′–c* conformation of α-maltose with respect to the value of 118.1°, at the lowest energy point (see Fig. 2a). (b) Relative H1–C1–O1 angle (°) as a function of (ϕ_H, ψ_H) for the *gg–gg′–c* conformation of α-maltose with respect to the value of 110.7°, at the lowest energy point (see Fig. 2a). (c) Relative H4′–C4′–O1 angle (°) as a function of (ϕ_H, ψ_H) for the *gg–gg′–c* conformation of α-maltose with respect to the value of 109.8°, at the lowest energy point (see Fig. 2a).

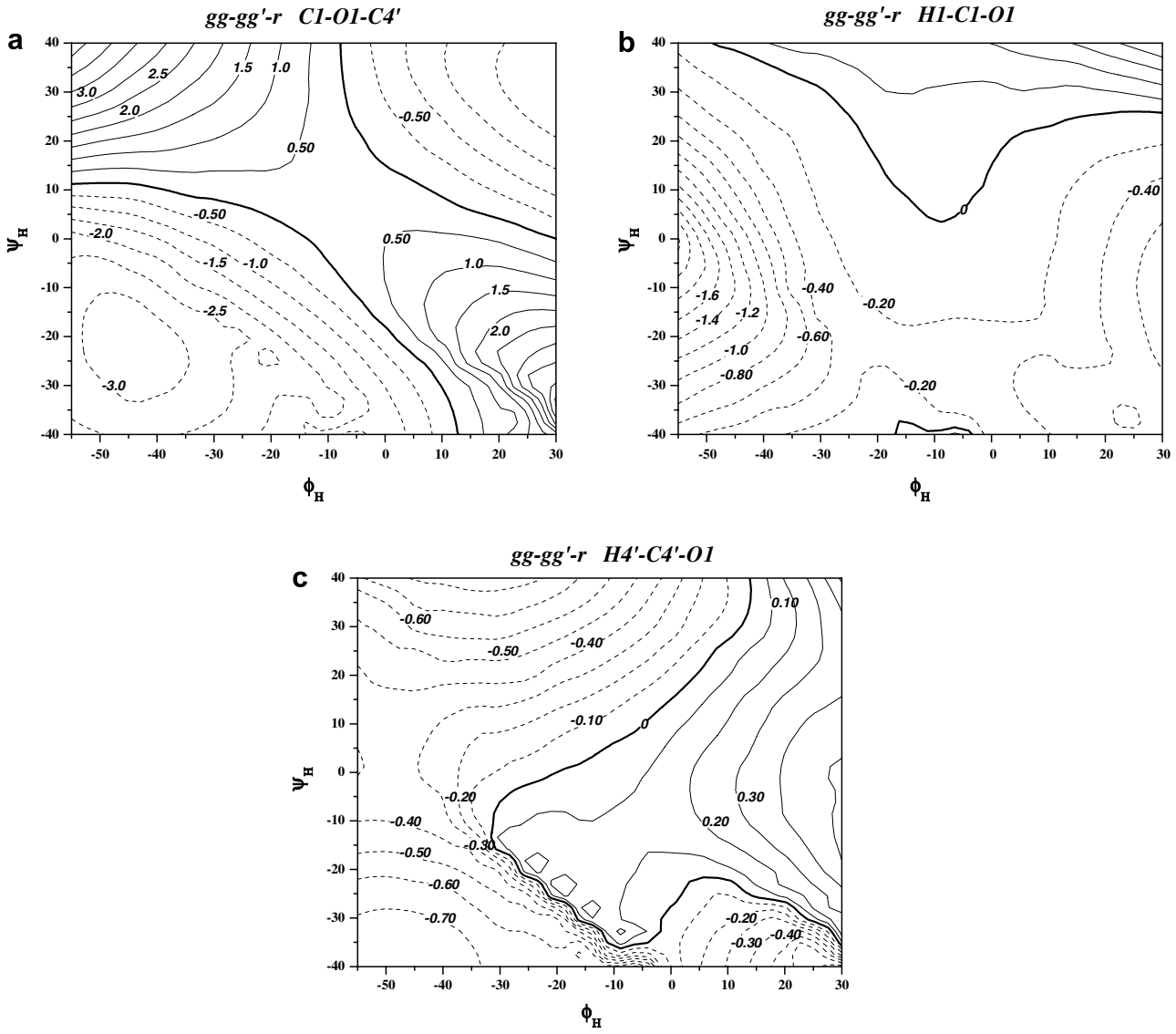

Figure 12. Isogeometric (ϕ,ψ) maps for the C1–O1–C4′, H1–C1–O1, and H4′–C4′–O1 angles. (a) Relative C1–O1–C4′ angle (°) as a function of (ϕ_H,ψ_H) for the *gg–gg′–r* conformation of α-maltose with respect to the value of 119.2°, at the lowest energy point (see Fig. 2a). (b) Relative H1–C1–O1 angle (°) as a function of (ϕ_H,ψ_H) for the *gg–gg′–r* conformation of α-maltose with respect to the value of 110.0°, at the lowest energy point (see Fig. 2a). (c) Relative H4′–C4′–O1 angle (°) as a function of (ϕ_H,ψ_H) for the *gg–gg′–r* conformation of α-maltose with respect to the value of 110.2°, at the lowest energy point (see Fig. 2a).

conformations, and with similar deviations of both positive and negative values of ∼2° at the extremes of the maps. The *gt–gt′–c* and *gt–gt′–r* maps for these angles appear very similar to those of the *gg–gg′–c* and *gg–gg′–r* forms shown, and are not presented here. Similarly, the *tg–tg′–c* and *tg–tg′–r* angle maps are similar to Figures 11 and 12, and differ only in the magnitude of change at the extremes, which are greater for the *tg* conformers. The *tg–tg′* bond angle maps are not shown.

In Figures 11a and 12a is shown the deviation in C1–O1–C4′ for the *gg–gg′–c* and '*r*' forms. The -0- deviation line in Figure 11a runs from ϕ_H ∼0° to ψ_H ∼0° in a diagonal way and again appears in the upper right-hand corner of the map. The lower -0- line runs through the low-energy conformation for the '*c*' form, while the upper line runs close to the minimum-energy conformation for the '*r*' form. For the most part, the deviations are small, of a few degrees with most of the map deviating less than 1 degree. The map for the '*r*' form is very similar with the -0- deviation line running through the low energy '*r*' minimum-energy position, and also following fairly closely the '*c*' minimum-energy position. The shapes of the two maps are closely similar, as one would expect.

Clearly, the variation in H1–C1–O1 bond angles (Figs. 11b and 12b) with the glycosidic dihedral angles is small, being of the order of less than ±0.2° in all the low-energy regions. If one superimposes the angle

variation maps with the isopotential maps, it is clear that the -0- deviation contour of the angle variation map passes through the low-energy space on the energy maps as it must, because of the base state chosen. These variances are also found for the *gt–gt'-c* and '*r*' conformers. It is apparent that there is little stress on these angles when the conformation is near its low-energy state.

The magnitudes of the H4′–C4′–O1 bond angle deviations shown for *gg–gg′–c* and *gg–gg′–r* in Figures 11c and 12c are similar to those for H1–C1–O1. The shapes of the H4′–C4′–O1 maps differ from one another since the directions that the cross-bridge hydroxyl groups make do change the variation of this bond angle somewhat more than that found in the previous H1–C1–O1 maps.

3.3. Non-bonded distances

Several non-bonded distances are of interest, having direct relationships to the stability of the different conformations. The distance across the hydrogen bond between H′(O3′) to O2, and between H(O2) to O3′ are of interest, as is the H1···H4′ distance across the glycosidic bonds. These coordinates are shown in Figure 13a for the *gg–gg′–c* and Figure 13b for the *gg–gg′–r* form. In Figure 13a the H′(O3′)···O2 distance is seen to remain relatively constant (2.4–2.9 Å) over a large variation in ϕ_H and ψ_H. Figure 13b also shows relatively a little variation in the H(O2)···O3′ distance when in the '*r*' form, assuming similar changes in glycosidic dihedral angles. It is of interest that the distances are generally shorter in the '*r*' form, except where the 'kink' conformer is found on the map. Of most interest is the observation that the H1···H4′ distance, Figure 13c, retains a value of ~2.15 Å over a rather large ϕ_H–ψ_H space. This distance is compatible with experimental NMR values as described in Ref. 1. It is not necessary to show the *gt–gt′* conformations as these coordinates are relatively independent of the hydroxymethyl rotamer type.

3.4. Dipole moments

Deviations of the dipole moments for the '*c*' and '*r*' forms of the different hydroxymethyl groups differ in their shapes although the magnitudes of the differences are very similar (see Fig. 14a–d). The largest deviations are of the order of ~0.5 D, with most of the ϕ_H–ψ_H maps landscape showing smaller variances. The -0- deviation contour line in the dipole maps follows generally

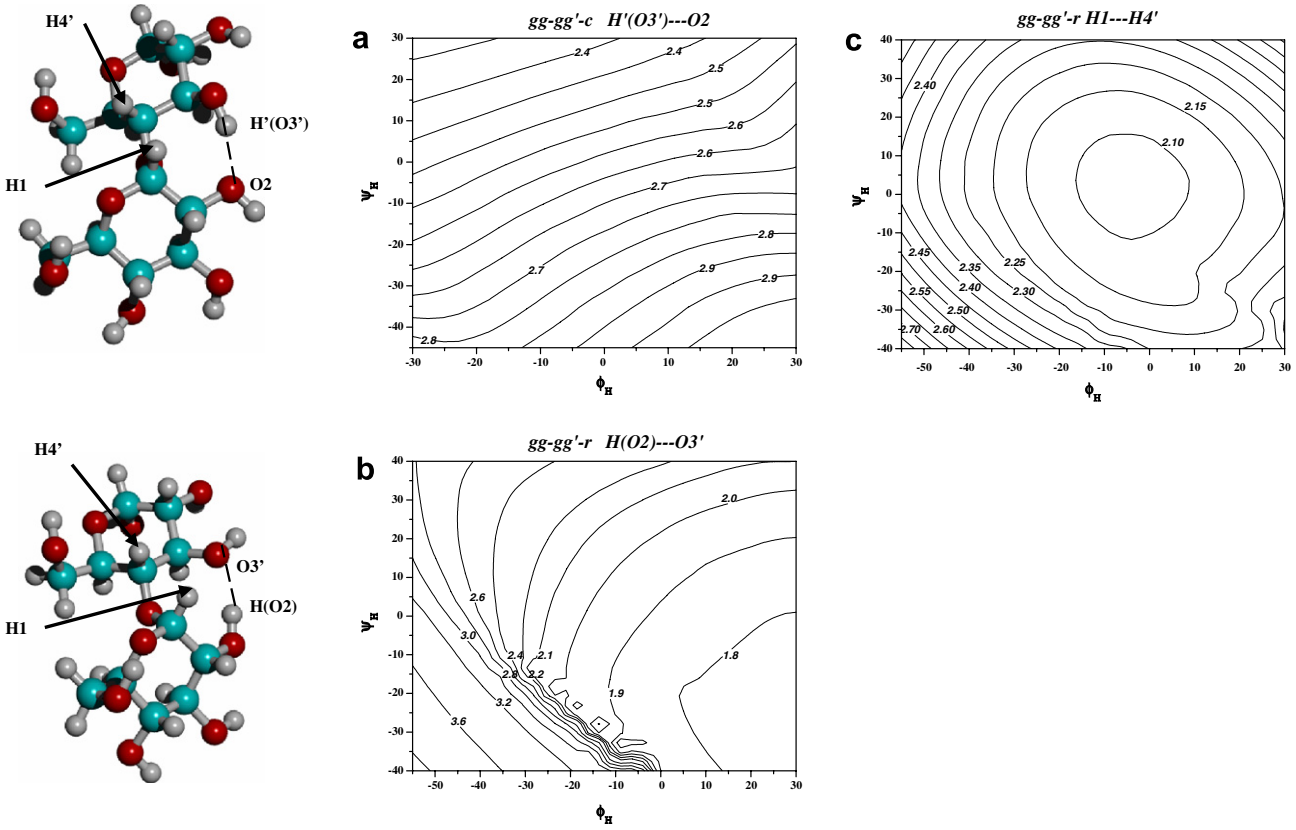

Figure 13. Isogeometric (ϕ_H, ψ_H) maps for the H′(O3′)···O2 and H(O2)···O3′ bond distances (Å) across the glycosidic bridge are shown in Figures a and b, for the *gg–gg′–c* and *gg–gg–r* conformer of α-maltose, respectively. Figure c shows the isogeometric (ϕ_H, ψ_H) map for the distance (Å) between the H1···H4′ hydrogen atoms of the *gg–gg′–r* conformer of α-maltose.

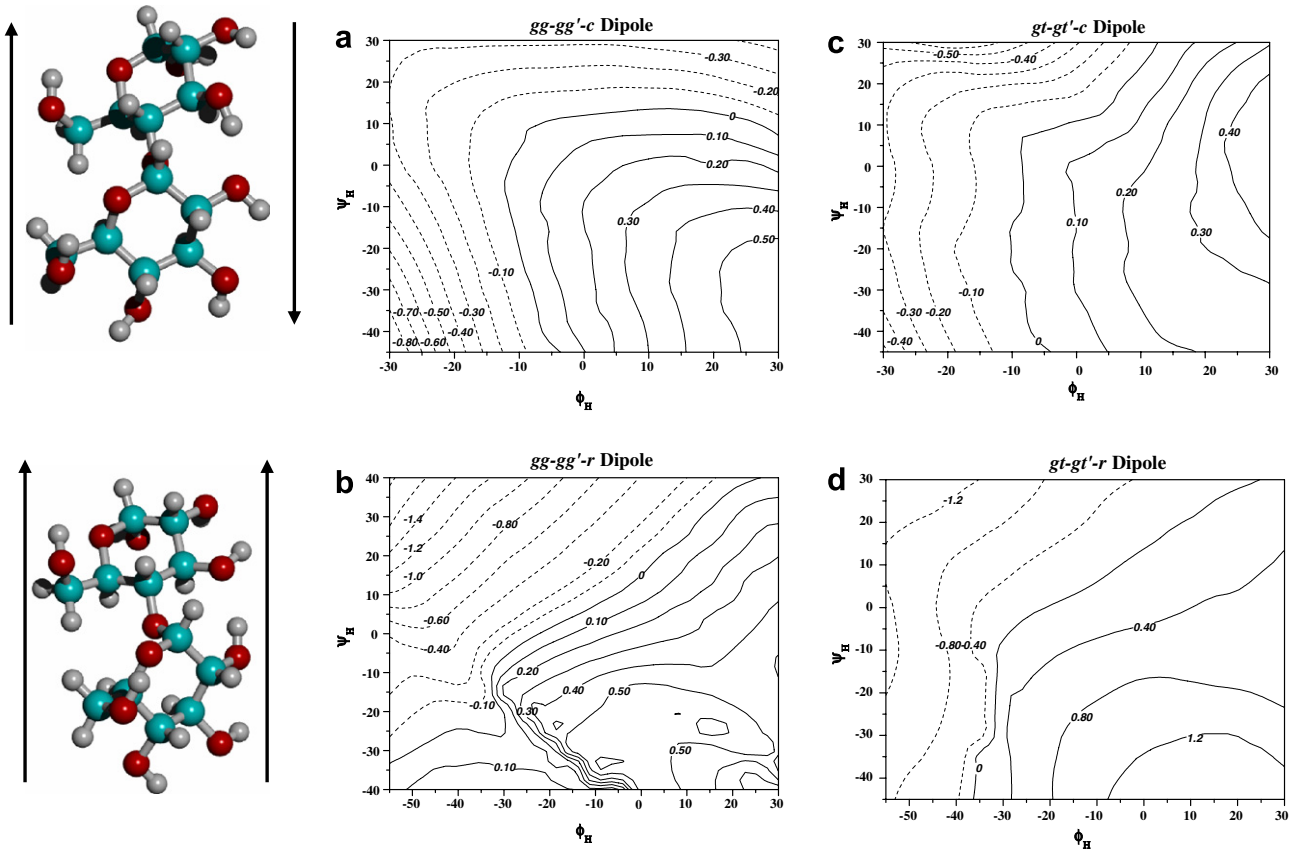

Figure 14. Dipole contour maps. (a) Relative dipole moment (Debye) as a function of (ϕ_H, ψ_H) for the *gg–gg′–c* conformation of α-maltose with respect to the dipole moment of 2.9 D at the lowest energy point (see Fig. 2a). (b) Relative dipole moment (Debye) as a function of (ϕ_H, ψ_H) for the *gg–gg′–r* conformation of α-maltose with respect to the dipole moment of 7.6 D at the lowest energy point (see Fig. 2b). (c) Relative dipole moment (Debye) as a function of (ϕ_H, ψ_H) for the *gt–gt′–c* conformation of α-maltose with respect to the dipole moment of 5.9 D at the lowest energy point (see Fig. 3a). (d) Relative dipole moment (Debye) as a function of (ϕ_H, ψ_H) for the *gt–gt′–r* conformation of α-maltose with respect to the dipole moment of 5.6 D at the lowest energy point (see Fig. 3b). The arrows at the shown α-maltose structures indicate the relative direction of the partial dipole moments along the sides of the molecule for the *gg–gg′–c* and *gg–gg′–r* conformers, respectively.

the shape of the energy isopotential contours, as one would anticipate from the orientation of the dipole moments. The zero deviation line in the '*c*' form passes through both the minimum-energy position of the *gg–gg′–c* conformation, but also passes through the energy minimum position of the *gg–gg′–r* form. The *gg–gg′–r* dipole deviation does not pass through the *gg–gg′–c* energy minimum position although it is not too far removed.

The magnitude of the dipole moments is of interest because the '*c*' forms are almost always smaller by ~50% than the '*r*' forms,[1] and of opposite direction. Considering the *gg–gg*' case, this difference in dipole moment arises from the orientation of the H(O6)–O6 and the equivalent primed bond relative to the directions of the H(O2)–O2 and H(O3)–O3 bonds and their primed equivalents. In the case of the *gg–gg′–c* form the dipoles of these two sets of bonds are pointed in opposite directions resulting in a small dipole moment, while in the *gg–gg′–r* form these bond dipoles are nearly parallel in direction and similar in magnitude, and the resulting molecular dipole moment is significantly larger. In the *tg* cases described next the H(O6)–O6 bond is nearly parallel to the 2-, and 3-position hydroxyl '*c*' forms, the '*r*' forms being antiparallel.

The dipole deviations for the *gt–gt′–c* and *gt–gt′–r* (Fig. 14c and d) are similar to the *gg–gg′–c* and '*r*' forms. Dipole deviations for the *tg–tg′–c* and *tg–tg′–r* conformations (Fig. 15a and b) are more dependent upon the close contact of the reducing residues hydroxymethyl when in the *tg* conformation. At larger deviations away from $(\phi_H, \psi_H) = \sim(0°, 0°)$, where the energy map also shows large deviations one finds large changes in the dipole moment. These arise because the large changes in hydroxymethyl dihedral angles change the bond dipole directions significantly.

4. Conclusions

There are many structural parameters one can observe from these mapping studies, a number of which have

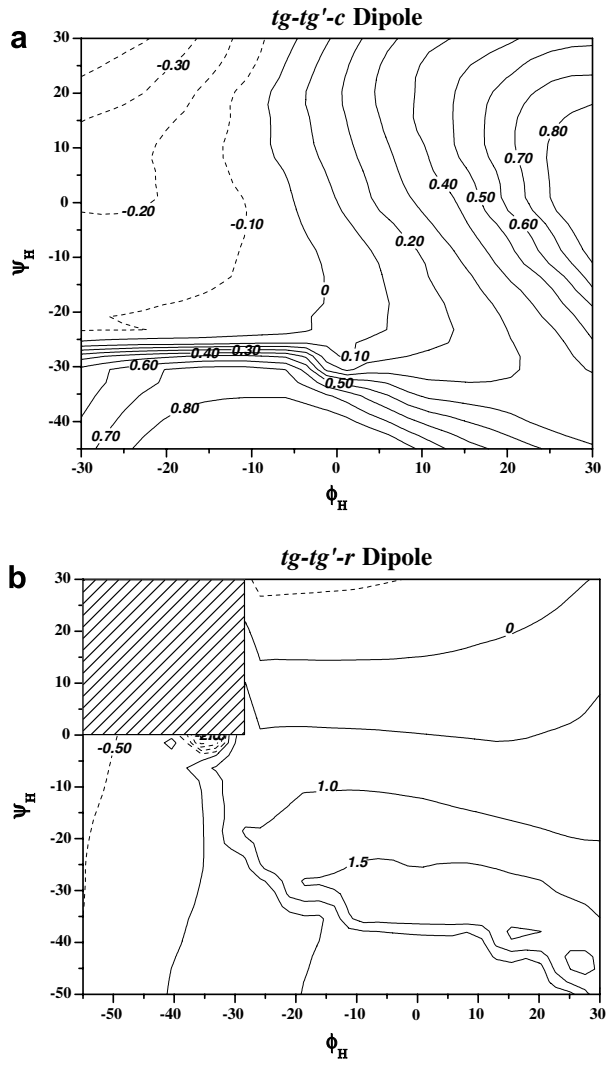

Figure 15. Dipole contour maps. (a) Relative dipole moment (Debye) as a function of (ϕ_H, ψ_H) for the *tg–tg′–c* conformation of α-maltose with respect to the dipole moment of 4.9 D at the lowest energy point (see Fig. 4a). (b) Relative dipole moment (Debye) as a function of (ϕ_H, ψ_H) for the *tg–tg′–r* conformation of α-maltose with respect to the dipole moment of 4.9 D at the lowest energy point (see Fig. 4b).

been described here. Of particular interest is the observation that for the most part, deviations from the optimum minimum-energy values are small until rather large variances from the energy minimum ϕ_H and ψ_H values, are made. Clearly, the energy landscape is rather soft (i.e., the energy gradient is small) around the minimum-energy regions, with deviations of one kcal/mol found only after moving more than $\sim(\pm 30°)$ in ϕ_H and ψ_H from the lowest energy positions. That this was found for all hydroxymethyl positions as well as for both '*c*' and '*r*' hydroxyl directions is of interest since it clearly establishes the considerable flexibility of the glycosidic bridge being rather independent of hydroxyl direction or hydroxymethyl conformations. There is also no ambiguity in the positions of the energy minima being directly related to the direction of the hydroxyl groups, the positions of energy minima being strongly dependent upon the '*c*' and '*r*' directions. This is totally consistent with the optimization studies recently published.[1] The area of the *gt–gt′–r* map inside the 1 kcal/mol contour is much larger than the *gg–gg′–r* area within the same contour, suggesting that the *gt–gt′–r* hydroxymethyl/hydroxyl conformation may be entropy preferred over the *gg–gg′* form. On the other hand, the area inside the 1 kcal/mol contour for the *gg–gg′–c* form appears to be larger than that in the *gt–gt′–c* form, again suggesting an entropy contribution favoring the former. This analysis must be compared with the absolute energies of the different minima.

The question of the average solution conformation remains to be determined, but preliminary studies using a dielectric solvent simulation method[27] while carrying out DFT molecular dynamics simulations on α-maltose, suggest that solvent does not significantly change the allowed regions of conformational space described here even though the pure '*c*' and '*r*' forms disappear and merge into new average structures during the dynamics.[28] Further, when larger amylose fragments (DP-3 and DP-4) are examined using the same computational tools used here and in previous calculations,[1,11–21] the energy difference between the '*c*' and '*r*' forms becomes more pronounced with the '*c*' conformers becoming significantly more stable than the '*r*' forms.[29]

References

1. Momany, F. A.; Schnupf, U.; Willett, J. L.; Bosma, W. B. *Struct. Chem.*, in press, doi: 10.1007/s11224-007-9191-9.
2. Ha, S. N.; Madson, L. J.; Brady, J. W. *Biopolymers* **1988**, *27*, 1927–1952.
3. Tran, V.; Buleon, A.; Imberty, A.; Pérez, S. *Biopolymers* **1989**, *28*, 679–690.
4. Dowd, M. K.; Zeng, J.; French, A. D.; Reilly, P. *J. Carbohydr. Res.* **1992**, *230*, 223–244.
5. Kouwijzer, M. L. C.; Grootenhuis, P. D. J. *J. Phys. Chem.* **1995**, *99*, 13426–13436.
6. Kuttel, M. M.; Naidoo, K. *J. Phys. Chem. B* **2005**, *109*, 7468–7474.
7. Stortz, C. A.; Cerezo, A. S. *J. Carbohydr. Chem.* **1998**, *17*, 1405–1419.
8. French, A. D.; Kelterer, A.-M.; Johnson, G. P.; Dowd, M. K.; Cramer, C. J. *J. Comput. Chem.* **2001**, *22*, 65–78.
9. da Silva, C. O.; Nascimento, M. A. C. *Carbohydr. Res.* **2004**, *339*, 113–122.
10. French, A. D.; Johnson, G. P.; Kelterer, A.-M.; Csonka, G. I. *Tetrahedron: Asymmetry* **2005**, *16*, 577–586.
11. Momany, F. A.; Willett, J. L. *J. Comput. Chem.* **2000**, *21*, 1204–1219.
12. Strati, G. L.; Willett, J. L.; Momany, F. A. *Carbohydr. Res.* **2002**, *337*, 1833–1849.
13. Strati, G. L.; Willett, J. L.; Momany, F. A. *Carbohydr. Res.* **2002**, *337*, 1851–1859.
14. Bosma, W. B.; Appell, M.; Willett, J. L.; Momany, F. A. J. *Mol. Struct.: THEOCHEM* **2006**, *776*, 1–19.

15. Bosma, W. B.; Appell, M.; Willett, J. L.; Momany, F. A. *J. Mol. Struct.: THEOCHEM* **2006**, *776*, 13–24.
16. Appell, M.; Strati, G. L.; Willett, J. L.; Momany, F. A. *Carbohydr. Res.* **2004**, *339*, 537–551.
17. Momany, F. A.; Appell, M.; Willett, J. L.; Schnupf, U.; Bosma, W. B. *Carbohydr. Res.* **2006**, *341*, 525–537.
18. Appell, M.; Willett, J. L.; Momany, F. A. *Carbohydr. Res.* **2005**, *340*, 459–468.
19. Schnupf, U.; Willett, J. L.; Bosma, W. B.; Momany, F. A. *Carbohydr. Res.* **2007**, *342*, 196–216.
20. Momany, F. A.; Appell, M.; Willett, J. L.; Bosma, W. B. *Carbohydr. Res.* **2005**, *340*, 1638–1655.
21. Momany, F. A.; Appell, M. A.; Strati, G. L.; Willett, J. L. *Carbohydr. Res.* **2004**, *339*, 553–567.
22. For the performance of B3LYP with a split valence basis set, see: (a) Novoa, J. J.; Sosa, C. J. *J. Phys. Chem.* **1995**, *99*, 15837–15845; Sirois, S.; Proynov, E. I.; Nguyen, D. T.; Salahub, D. R. *J. Chem. Phys.* **1997**, *107*, 6770–6781; Paizs, B.; Suhai, S. *J. Comput. Chem.* **1998**, *19*, 575–584; Hagemeister, F. C.; Gruenloh, C. J.; Zwier, T. S. *J. Phys. Chem. A* **1998**, *102*, 82–94.
23. PQS 3.2 Ab Initio Program Package, Parallel Quantum Solutions, Fayetteville, AR.
24. HYPERCHEM 7.5, Hypercube, Gainesville, FL.
25. ORIGIN 7.5, OriginLab Corporation, Northampton, MA.
26. French, A. D.; Kelterer, A.-M.; Johnson, G. P.; Dowd, M. K.; Cramer, C. J. J. *Mol. Graph. Model.* **2000**, *18*, 95–107.
27. Klamt, A.; Schuurmann, G. J. *J. Chem. Soc., Perkin Trans. 2.* **1993**, *5*, 799–805.
28. Momany, F. A.; Willett, J. L.; Bosma, W. B.; Schnupf, U. *Abstracts of Papers*, 233rd ACS National Meeting, Chicago, IL, March 25–29, 2007; American Chemical Society: Washington, DC, 2007, COMP-58.
29. Schnupf, U.; Momany, F. A.; Willett, J. L.; Bosma, W. B. *Abstracts of Papers*, 232nd ACS National Meeting, San Francisco, CA, September 10–14, 2006; American Chemical Society: Washington, DC, 2006, CARB-105.